# Spectra Estimation of Fluorescent and Reflective Scenes by Using Ordinary Illuminants

Yinqiang Zheng[1], Imari Sato[1], and Yoichi Sato[2]

[1] National Institute of Informatics, Japan
[2] The University of Tokyo, Japan
{yqzheng,imarik}@nii.ac.jp, ysato@iis.u-tokyo.ac.jp

**Abstract.** The spectrum behavior of a typical fluorescent object is regulated by its reflectance, absorption and emission spectra. It was shown that two high-frequency and complementary illuminations in the spectral domain can be used to simultaneously estimate reflectance and emission spectra. In spite of its accuracy, such specialized illuminations are not easily accessible. This motivates us to explore the feasibility of using ordinary illuminants to achieve this task with comparable accuracy. We show that three hyperspectral images under wideband and independent illuminants are both necessary and sufficient, and successfully develop a convex optimization method for solving. We also disclose the reason why using one or two images is inadequate, although embedding the linear low-dimensional models of reflectance and emission would lead to an apparently overconstrained equation system. In addition, we propose a novel four-parameter model to express absorption and emission spectra, which is more compact and discriminative than the linear model. Based on this model, we present an absorption spectra estimation method in the presence of three illuminations. The correctness and accuracy of our proposed model and methods have been verified.

**Keywords:** Fluorescence, reflectance, hyperspectral imaging.

## 1 Introduction

Recently, fluorescence has aroused much interest in the computer vision community, due to its quite special Stokes wavelength shift effect and its color invariance under varying spectra illuminations [23]. Specifically, as an inherent physical property, a pure fluorescent object would absorb energy in a certain wavelength range, and re-emit it in a longer (or more exactly, redder) wavelength range. Irrespective of the illumination spectra, the spectra distribution of emission keeps constant except its magnitude.

The necessity of accounting for fluorescence has been justified in computational color constancy [4] and accurate color relighting [9, 11, 13], when nontrivial fluorescent components are present in the scene. Its unique spectral properties have also facilitated some important applications. For example, the wavelength shift effect was utilized to suppress highlights and inter-reflections in photometric stereo [19, 22], while the color invariance used in [10] for camera spectral sensitivity calibration. These applications and perhaps more in prospect warrant the ongoing endeavors of exploring fluorescence.

However, a typical fluorescent object is usually a composite of reflective and fluorescent components. The reflective component reflects back the irradiance at the same

D. Fleet et al. (Eds.): ECCV 2014, Part V, LNCS 8693, pp. 188–202, 2014.


(a) Illuminants (b) Spectra (c) Scene (LED) (d) Reflectance (e) Fluorescence

**Fig. 1.** Using ordinary illuminants for fluorescence and reflectance separation. (a) shows the three incandescent, LED and fluorescent bulbs used in the experiments on real images, whose spectra are presented in (b). The scene under LED is shown in (c), and its recovered reflective and fluorescent components are given in (d) and (e), respectively.

wavelength, thus interacting with the illuminant quite differently from the fluorescent component. It is therefore the prerequisite to segment the fluorescent from the reflective component (see Fig.1(c-e) for an example). Some existing works have achieved solid progress toward this end in RGB images. Zhang and Sato [23] separated these two components under two different illuminations by means of independent component analysis. In contrast, Han et al. [10] used a single RGB image with the assistance of a reflectance color checker.

As demonstrated in those works on reflectance-only scenes, like [7, 12, 17] and many others, multispectral or hyperspectral information is essential in scenarios where color accuracy takes precedence, such as high-definition color production and e-heritage archiving. Similarly, when dealing with a fluorescent-reflective scene, it would be more desirable to recover the full spectra information, rather than being satisfied with the RGB color only. In the following, we briefly review the most closely related works on fluorescence-reflectance spectra estimation.

### 1.1 Related Works on Fluorescence Spectra Estimation

Some researchers have tried to recover the spectra of fluorescence. For example, Tominaga et al. [21] adopted two different light sources to estimate the fluorescent emission spectra. Alterman et al. [1] tried to unmix multiplexed images and obtain the appearance of individual fluorescent dye, while Boyd et al. [5] estimated the reflectance and fluorescent emission spectra of coral, without recovering the absorption spectra. In all these works, only a portion of the spectra are recovered.

Actually, reflectance and fluorescent emission are naturally detached under narrowband illuminations. Rooted in this observation, the classical bispectral method for full spectra measurement is widely known, and has been well documented in the literature [14]. However, this bispectral method in its original form is very laborsome and thus appropriate to measure a single point only. Lam and Sato [13] successfully extended it to measure a whole scene by using a monochromatic camera and a programmable filter. Similar to reflectance [15, 18], it was noted therein that the fluorescent emission and absorption can also be well represented by the linear subspace models, which are usually leaned from principle component analysis (PCA) of training data. Such PCA-based linear models were utilized in [13] to reduce the number of images. In spite of that, about 30 images are necessary to estimate the complete spectra of a fluorescence-reflectance scene.

The classical bispectral method also links directly to the latest bispectral coding scheme [20], which used multiplexed narrowband illuminations and images to recover the full spectra of a fluorescent-reflective scene.

Instead of capturing dozens of images, Fu et al. [9] proposed an appealing method to separate the reflective and fluorescent components of a scene by using two hyperspectral images taken under high-frequency and complementary illuminations in the spectral domain. Although it is highly accurate and convenient, to generate high-frequency illuminations requires some specialized devices, like a programmable lighting source, which are very expensive thus not widely available. As for absorption spectra estimation, they developed a data driven method under the assumption that the emission and absorption spectra have the same basis coefficients. As a result, the recovered absorption spectra assume nontrivial error, when the underlying assumption is violated.

In a similar spirit to our work, Fu et al. [8] tried to simplify the hardware setup of [9] by using instead multiple colored illuminations and a trichromatic camera. Compared with a hyperspectral camera, a RGB camera is definitely desirable in terms of cost reduction, yet tends to undermine the estimation accuracy of emission spectra due to the classical metamerism hurdle in recovering spectra from trichromatic values. In addition, the colored illumination spectra were still generated by a programmable lighting source therein.

### 1.2 Overview of This Work

Rather than relying on specialized narrowband or high-frequency illuminations, we aim to propose a new method for fluorescence and reflectance separation by using such ordinary illuminants as LED bulbs and fluorescent lamps (see Fig.1(a-b) for the three illuminants used in the experiments of this paper), without sacrificing accuracy nor increasing much human workload. We show that three hyperspectral images under arbitrarily independent illuminations are both necessary and sufficient to this task. Actually, due to linear dependence between the PCA-based linear model of reflectance and that of emission, using one or two images tends to be inaccurate, although embedding the linear models into the imaging equation would lead to an apparently overconstrained system. However, using three images would result in a nonconvex bilinear programming problem, which is challenging to solve in general. Fortunately, through proper transformation, we successfully reformulate it into an elegant linear system. On the basis of this system, we develop a convex optimization method, whose solution can be further polished via a few alternating iterations. Experiments on simulated data have verified that our proposed method is as accurate as the state-of-the-art method [9], although only ordinary illuminants are used. Our method has also been demonstrated to be effective by using real images.

Since the absorption can not be directly observed in the image, we have to estimate it in an indirect way. To facilitate this task, we propose instead a four-parameter nonlinear model to represent the emission and absorption spectra, which is much more compact than the well-known PCA-based linear model, yet assumes almost comparable representation power. Our inspiration is drawn from the observation that shapes of typical emission and absorption spectra are very similar to the density function of the skew Cauchy distribution [2, 3]. Relying on this model and the similarity between the

emission and absorption spectra pair, we develop a new method for absorption spectra estimation in the presence of three images, which is clearly advantageous in accuracy over the heuristic method in [9].

To sum up, our major contributions are: (i). Revealing for the first time the linear dependence between the PCA-based linear models of reflectance and emission; (ii). Deriving an elegant linear system for the imaging equations in the presence of three hyperspectral images; (iii). Developing an effective method to separate fluorescent and reflective components by using ordinary illuminants; (iv). Proposing a novel four-parameter nonlinear model to parameterize emission and absorption spectra on the basis of the skew Cauchy distribution.

The remaining parts of this paper are organized as follows. In Sec.2, we show how to separate the reflectance and fluorescent emission by using ordinary spectra illuminations. Sec.3 includes the four-parameter nonlinear model for representing emission and absorption spectra as well as the absorption spectra estimation method. We present experiment results by using simulated data and real images in Sec.4, and briefly conclude this paper in Sec.5.

## 2 Reflectance and Emission Spectra Separation

As mentioned above, a typical fluorescent object exhibits the mixed spectrum behavior of reflectance and fluorescence. According to [9, 23], the radiance at wavelength $\lambda$ of a pure reflective surface is computed as $l(\lambda)r(\lambda)$, in which $l(\lambda)$ is the illumination spectra and $r(\lambda)$ is the reflectance spectra. In contrast, due to the particular absorption-emission mechanism, the radiance of a pure fluorescent surface is regulated by $\left(\int l(\hat{\lambda})a(\hat{\lambda})d\hat{\lambda}\right)e(\lambda)$, in which $a(\lambda)$ and $e(\lambda)$ are the absorption and emission spectra, respectively. Therefore, the total radiance $p(\lambda)$ of a fluorescent-reflective surface can be calculated by the following imaging equation

$$p(\lambda) = l(\lambda)r(\lambda) + \left(\int l(\hat{\lambda})a(\hat{\lambda})d\hat{\lambda}\right)e(\lambda). \tag{1}$$

Note that the absorption spectra $a(\lambda)$ is merged into a scalar coefficient of emission, i.e. $\int l(\hat{\lambda})a(\hat{\lambda})d\hat{\lambda}$, thus it could not be directly observed in the radiance $p(\lambda)$. Therefore, the full spectra estimation problem is usually formulated as a separation problem of reflectance and fluorescent emission at the first stage.

Rather than using specialized narrowband or high-frequency illuminations, we aim at achieving this separation task by using ordinary illuminants. As shall be disclosed later, we have found that, by using three hyperspectral images, the separation is feasible under the mild assumption that the three illumination spectra are wideband and mutually independent. This mild condition allows us to use such ordinary illuminants in daily life as LED bulbs and fluorescent lamps.

### 2.1 Using Three Hyperspectral Images

Given three illumination spectra $l_j(\lambda)$ and their corresponding radiance $p_j(\lambda)$ recorded by a hypersepctral camera with $n$ bands, the imaging equation in eq.(1) can be rewritten as

$$p_j(\lambda_i) = l_j(\lambda_i)r(\lambda_i) + a_j e(\lambda_i), i = 1, 2, \cdots, n, j = 1, 2, 3, \tag{2}$$

where the scalar $a_j$ is introduced to represent the absorption coefficient $\int l_j(\hat{\lambda})a(\hat{\lambda})d\hat{\lambda}$. Due to the scale ambiguity between $a_j$ and $e$, without loss of generality, we can simply introduce a scale constraint such that $a_1 + a_2 + a_3 = 1$. It causes no problem since $a_1$, $a_2$ and $a_3$ are positive for an excited fluorescent-reflective object.

Apparently, the three equations in eq.(2) provide $3n + 1$ constraints, one of which is the scale constraint $a_1 + a_2 + a_3 = 1$ that we have introduced. The number of variables is $2n + 3$. It seems to tell that using three images would result in an overconstrained system, without involving any low-dimensional models of reflectance and emission. To obtain the reflectance and emission spectra, we need to solve the following bilinear programming problem

$$\min_{a_j, \mathbf{r}, \mathbf{e}} \quad \left\| \begin{bmatrix} L_1 & A_1 \\ L_2 & A_2 \\ L_3 & A_3 \end{bmatrix} \begin{bmatrix} \mathbf{r} \\ \mathbf{e} \end{bmatrix} - \begin{bmatrix} \mathbf{p}_1 \\ \mathbf{p}_2 \\ \mathbf{p}_3 \end{bmatrix} \right\|_2^2, s.t., \sum_{j=1}^{3} a_j = 1, a_j \geq 0, \mathbf{r} \geq \mathbf{0}, \mathbf{e} \geq \mathbf{0}, \tag{3}$$

in which $L_j$, $j = 1, 2, 3$, represents $diag\{l_j(\lambda_1), \cdots, l_j(\lambda_n)\}$, while $A_j$ denotes the diagonal matrix of $a_j$. In addition, $\mathbf{p}_j = \left[p_j(\lambda_1), \cdots, p_j(\lambda_n)\right]^T$, $\mathbf{r} = \left[r(\lambda_1), \cdots, r(\lambda_n)\right]^T$ and $\mathbf{e} = \left[e(\lambda_1), \cdots, e(\lambda_n)\right]^T$.

The optimization problem in eq.(3) is very challenging due to its nonconvexity, arising from the bilinear correlation between $a_j$ and $\mathbf{e}$. We can retrieve its global minimum by using two-dimensional exhaustive search, which is extremely slow. In contrast, using certain local optimization method would require a reasonable initialization, which is unknown yet. In the following, we reformulate the imaging equations into a linear system, which in turn clearly reveals the condition on the illumination spectra for solution uniqueness.

### 2.2 Reformulation and Practical Algorithm

For the current time being, let us assume that the absorption scalars $a_1$, $a_2$ and $a_3$ are known. Then, the first two equations in eq.(2) happen to have the same number ($2n$) of constraints and variables, from which the reflectance $r(\lambda_i)$ and the emission $e(\lambda_i)$ can be solved in closed form as

$$r(\lambda_i) = \frac{a_2 p_1(\lambda_i) - a_1 p_2(\lambda_i)}{a_2 l_1(\lambda_i) - a_1 l_2(\lambda_i)}, e(\lambda_i) = \frac{p_2(\lambda_i) l_1(\lambda_i) - p_1(\lambda_i) l_2(\lambda_i)}{a_2 l_1(\lambda_i) - a_1 l_2(\lambda_i)}. \tag{4}$$

After plugging eq.(4) into the third equation of eq.(2), we obtain

$$p_3(\lambda_i) = \frac{l_3(\lambda_i)\left[a_2 p_1(\lambda_i) - a_1 p_2(\lambda_i)\right] + a_3\left[p_2(\lambda_i) l_1(\lambda_i) - p_1(\lambda_i) l_2(\lambda_i)\right]}{a_2 l_1(\lambda_i) - a_1 l_2(\lambda_i)}. \tag{5}$$

By multiplying the denominator $a_2 l_1(\lambda_i) - a_1 l_2(\lambda_i)$ at both sides of eq.(5), a very compact linear equation can be obtained after some basic algebraic operations

$$\left[p_2 l_3 - p_3 l_2 \;\; p_3 l_1 - p_1 l_3 \;\; p_1 l_2 - p_2 l_1\right]\left[a_1 \; a_2 \; a_3\right]^T = 0, \tag{6}$$

in which the wavelength index $\lambda_i$ has been omitted for brevity. Therefore, all $n$ bands can be stacked into a matrix form

$$\left[\mathbf{p}_2 \odot \mathbf{l}_3 - \mathbf{p}_3 \odot \mathbf{l}_2 \;\; \mathbf{p}_3 \odot \mathbf{l}_1 - \mathbf{p}_1 \odot \mathbf{l}_3 \;\; \mathbf{p}_1 \odot \mathbf{l}_2 - \mathbf{p}_2 \odot \mathbf{l}_1\right] \begin{bmatrix} a_1 \\ a_2 \\ a_3 \end{bmatrix} = M \begin{bmatrix} a_1 \\ a_2 \\ a_3 \end{bmatrix} = \mathbf{0}, \tag{7}$$

where the operator $\odot$ denotes element-wise multiplication of vectors. $M$ is the $n \times 3$ data matrix constructed from the radiance vectors $\mathbf{p}_j$ and illumination spectra vectors $\mathbf{l}_j$, $j = 1, 2, 3$.

In the noise-free case, eq.(7) has a unique solution, as long as the rank of $M$ is 2. This condition can be easily satisfied when the three illumination spectra are wideband and independent.

In presence of image noise, the rank of $M$ is usually 3. Based on eq.(7), we can easily estimate the absorption scalars by solving the following convex quadratic program

$$\min_{a_1,a_2,a_3} \quad \left\| M \left[a_1 \; a_2 \; a_3\right]^T \right\|_2^2, s.t., a_1 + a_2 + a_3 = 1, a_1 \geq 0, a_2 \geq 0, a_3 \geq 0. \tag{8}$$

In the derivation process of eq.(6), the three images are not treated in a balanced manner, that is, to explicitly build the linear system on the third image, while using the first and second images to solve the reflectance and emission spectra. In addition, the nonnegative constraints of reflectance and emission spectra have been ignored. To further improve accuracy, we can start from the solution from eq.(8), and minimize eq.(3) via the standard alternating minimization scheme. Specifically, given $a_1$, $a_2$ and $a_3$, all $n$ bands become independent, thus we can easily update $r(\lambda_i)$ and $e(\lambda_i), i = 1, 2, \cdots, n$, by solving $n$ trivial quadratic programs

$$\min_{r(\lambda_i),e(\lambda_i)} \quad \left\| \begin{bmatrix} l_1(\lambda_i)\; a_1 \\ l_2(\lambda_i)\; a_2 \\ l_3(\lambda_i)\; a_3 \end{bmatrix} \begin{bmatrix} r(\lambda_i) \\ e(\lambda_i) \end{bmatrix} - \begin{bmatrix} p_1(\lambda_i) \\ p_2(\lambda_i) \\ p_3(\lambda_i) \end{bmatrix} \right\|_2^2, s.t., r(\lambda_i) \geq 0, e(\lambda_i) \geq 0. \tag{9}$$

When $r(\lambda_i)$ and $e(\lambda_i), i = 1, 2, \cdots, n$, are known, $a_1$, $a_2$ and $a_3$ can be updated by solving

$$\min_{a_1,a_2,a_3} \quad \left\| \begin{bmatrix} \mathbf{e} & & \\ & \mathbf{e} & \\ & & \mathbf{e} \end{bmatrix} \begin{bmatrix} a_1 \\ a_2 \\ a_3 \end{bmatrix} - \begin{bmatrix} \mathbf{p}_1 - \mathbf{l}_1 \odot \mathbf{r} \\ \mathbf{p}_2 - \mathbf{l}_2 \odot \mathbf{r} \\ \mathbf{p}_3 - \mathbf{l}_3 \odot \mathbf{r} \end{bmatrix} \right\|_2^2, s.t., a_1 + a_2 + a_3 = 1, a_1 \geq 0, a_2 \geq 0, a_3 \geq 0. \tag{10}$$

Since the initialization from solving eq.(8) is already sufficiently accurate, the maximum iteration number of alternating minimization is chosen to be 10 in all the experiments. In addition, it is well known that a small convex quadratic program with simple bound constraints can be directly solved via the active set method. Therefore, we can solve all the programs in eq.(8), eq.(9) and eq.(10) efficiently by using linear algebraic operations in closed form, rather than resorting to the more complicated iterative interior point method [6].

To sum up, the procedures of our algorithm for reflectance and fluorescent emission separation are: (i). Constructing the data matrix $M$ in eq.(7); (ii). Solving eq.(8) to obtain the absorption scalars $a_1$, $a_2$ and $a_3$; (iii). Solving eq.(9) and eq.(10) alternatively to

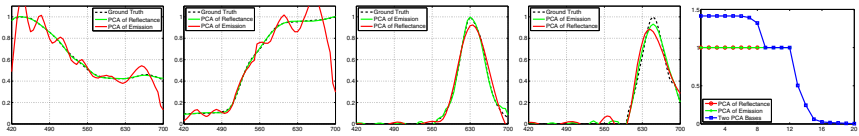


(a) Ref.-1 (b) Ref.-2 (c) Emi.-1 (d) Emi.-2 (e) SV

**Fig. 2.** Dependence between the reflectance and the emission PCA bases. (a) and (b) show that a reflectance spectra can be well approximated by the emission bases, while (c) and (d) illustrate that the reflectance bases can approximate the emission spectra as well. The reason lies in the linear dependence between these two bases, as verified by their singular values (SV) in (e).

refine the estimation of the reflectance $r(\lambda_i)$ and the emission $e(\lambda_i), i = 1, 2, \cdots, n$, until the maximum number of iterations (10 in our experiments) is reached. To deal with a fluorescent-reflective scene, one should repeat the above procedures for all pixels in the scene. Due to this pixel-wise independence, the whole algorithm can be easily parallelized for faster speed.

Until now, we have shown that using three hyperspectral images under mild restrictions on the illumination spectra is sufficient for fluorescent and reflective spectra separation. In the following, we explore the possibility of reducing the number of images further.

### 2.3 Using One or Two Images

Given a single hyperspectral image, we have only the first equation of eq.(2) at hand

$$p_1(\lambda_i) = l_1(\lambda_i)r(\lambda_i) + a_1 e(\lambda_i), i = 1, 2, \cdots, n. \tag{11}$$

Here, to resolve the ambiguity between $a_1$ and $e$, we can assume that $a_1 = 1$. Therefore, eq.(11) has $2n$ variables and $n$ constraints, and as a result infinitely many solutions.

It has long been known that practical reflectance can be well represented by a linear model with low dimensionality, e.g. 8, as verified in [15, 18]. Lam and Sato [13] observed that the fluorescent emission can also be accurately approximated by using a 12-D linear model leaned from PCA of training data. In order to reduce the number of variables, a straightforward idea is to embed the linear models into eq.(11) as follows

$$\mathbf{p}_1 = L_1\mathbf{r} + \mathbf{e} = L_1 B_r \mathbf{c}_r + B_e \mathbf{c}_e. \tag{12}$$

At first glance, eq.(12) is overconstrained, since the number of constraints is $n$, which is usually much larger than the total number of bases (8+12=20). The coefficients $\mathbf{c}_r$ and $\mathbf{c}_e$ can be obtained by solving the following convex quadratic program

$$\min_{\mathbf{c}_r, \mathbf{c}_e} \left\| \begin{bmatrix} L_1 B_r & B_e \end{bmatrix} \begin{bmatrix} \mathbf{c}_r \\ \mathbf{c}_e \end{bmatrix} - \mathbf{p}_1 \right\|_2^2, s.t., B_r\mathbf{c}_r \geq \mathbf{0}, B_e\mathbf{c}_e \geq \mathbf{0}, \tag{13}$$

into which we have incorporated the nonnegative constraints of reflectance and emission.

However, our experiment results, as shall be shown in Fig.5, reveal that the estimation accuracy of reflectance and emission is very poor even in no presence of image

noise. By closer investigation, we have found that the primary reason lies in the linear dependence of the bases of reflectance and emission. Specifically, as shown in Fig.2, although the PCA-based linear model of reflectance can express a reflectance spectra exactly, it can also approximate emission with reasonable accuracy, and vice versa. This dependence is more obvious when observing the singular values of these two bases in Fig.2(e). We have also observed that simply reducing the number of bases, surely at the cost of weakening expression power, would rarely remedy this dependence problem.

How about using two images? Given the second illumination spectra $l_2(\lambda)$ and its corresponding radiance $p_2(\lambda)$, the second equation in eq.(2) reads

$$p_2(\lambda_i) = l_2(\lambda_i)r(\lambda_i) + a_2 e(\lambda_i), i = 1, 2, \cdots, n. \tag{14}$$

To fix the scale ambiguity of $a_1$ and $a_2$, we add a scale constraint such that $a_1 + a_2 = 1$.

Again, eq.(11) and eq.(14) offer $2n + 1$ constraints, thus less than the number of variables $2n + 2$. One possible way is to introduce the linear models for reflectance and emission, which still suffers from the basis dependence problem, as shall be shown in Fig.5(b-c). Note that, in the solving process, we conduct one-dimensional search over $a_1$ to make sure that the globally optimal solution is retrieved, although eq.(11) and eq.(14) are bilinear in terms of $a_1$, $a_2$ and $e(\lambda_i)$.

Using high-frequency illuminations [9] can be interpreted as another remedy, since the absorption scalars $a_1$ and $a_2$ tend to be equal under high-frequency and complementary illuminations. In effect, it adds another constraint $a_1 = a_2$, and makes eq.(11) and eq.(14) uniquely solvable. Unfortunately, this equality does not hold under ordinary illuminations.

One might consider to use RGB images, instead of hyperspectral images, so as to further reduce the cost. Unfortunately, when using RGB images, one illumination offers only three constraints, such a separation method would rely heavily on the subspace model to reduce the number of variables, and consequently, should be more likely to suffer from the aforementioned linear dependence problem.

One might also wonder why using the linear subspace models caused no problem in [13]. Let us recall that narrowband illuminations were used there. Under this condition, reflectance and fluorescence are almost detached, because of the wavelength shift effect. Therefore, the work [13] is more about spectra fitting of individual components than on spectra separation.

## 3 Absorption Spectra Estimation

In this section, we show how to estimate the absorption spectra $a(\lambda_i), i = 1, 2, \cdots, n$, by using the three absorption scalars $a_1$, $a_2$, $a_3$, as well as the estimated emission spectra $e(\lambda_i)$. Note that the aforementioned linear model in [13] is inapplicable to our setup, since its dimensionality is much larger than the number of constraints that we have at hand.

As shown in Fig.3(a), the absorption and emission spectra pair of a typical fluorescent material have bell-like shapes, with a long tail toward the short-wavelength and the long-wavelength direction, respectively. This is very similar to the density function of the skew Cauchy distribution, as shown in Fig.3(b-d). This observation motivates us to develop a compact low-dimensional representation of absorption and emission spectra.

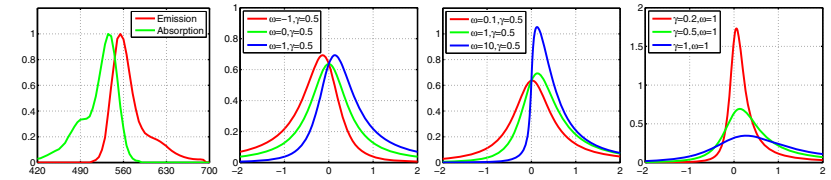


(a) Abs.&Emi. Pair (b) Skew Direction (c) Skew Magnitude (d) Width

**Fig. 3.** The absorption and emission spectra pair of a typical fluorescent material (a) v.s. the density function of the skew Cauchy distribution, with varying tail direction (b), skewness magnitude (c) and width (d).

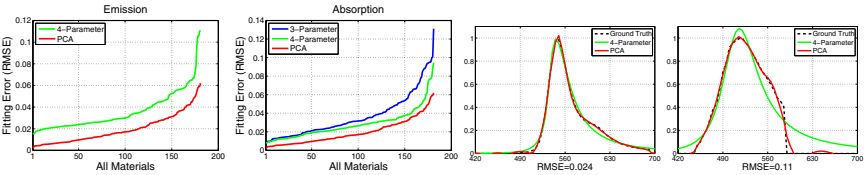


(a) Sorted Emi. RMSE (b) Sorted Abs. RMSE (c) Emi. 4-P (50th) (d) Emi. 4-P (181th)

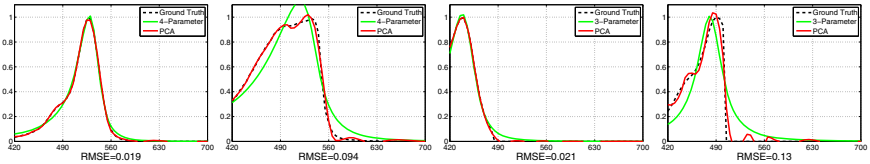


(e) Abs. 4-P (50th) (f) Abs. 4-P (181th) (g) Abs. 3-P (50th) (h) Abs. 3-P (181th)

**Fig. 4.** Verification of the four-parameter (4-P) and three-parameter (3-P) nonlinear models. (a) and (b) show the sorted fitting error (RMSE) of all 181 materials for emission and absorption spectra, respectively. Some examples of reasonable fitting (50th) and worst fitting (181th) are shown in (c-h).

### 3.1 Four-Parameter Nonlinear Model

Being a variant of the standard Cauchy distribution, the skew Cauchy distribution has a skewness parameter to control the magnitude and direction of its skew tail. The analytic form of its density function reads [2, 3]

$$f(x|x_0,\gamma,\omega) = \frac{\gamma}{\pi\left[\gamma^2+(x-x_0)^2\right]}\left\{\frac{1}{\pi}\arctan\left[\frac{\omega(x-x_0)}{\gamma}\right]+\frac{1}{2}\right\}, x\in\mathbb{R}, \qquad (15)$$

where $x_0$, $\gamma$ and $\omega$ are the location, width and skewness parameter, respectively. The skew Cauchy distribution is a special case of the skew $t$-distribution, when the number of degrees of freedom (DoF) is 1. When the DoF approaches infinity, the skew $t$-distribution reduces to the well-known skew normal distribution [3]. We prefer the skew Cauchy distribution because of its relatively simple analytical form.

An important property by observing Fig.3 is that the tail is toward to the left when $\omega < 0$, while to the right when $\omega > 0$. In addition, the skew magnitude is determined by the absolute value of $\omega$. This property actually allows us to explicitly discriminate the absorption spectra from the emission spectra.

In order to express the fluorescent emission and absorption, we introduce a height parameter $h$ and obtain the ultimate four-parameter model

$$f(x|x_0,\gamma,\omega,h) = \frac{h}{\left[\gamma^2+(x-x_0)^2\right]}\left\{\frac{1}{\pi}\arctan\left[\frac{\omega(x-x_0)}{\gamma}\right]+\frac{1}{2}\right\}. \tag{16}$$

To verify the validity of our proposed model, we have tried to fit it to the fluorescence spectra dataset [16] with 181 fluorescent materials in the visible range from 420 nm to 700 nm with an increment of 5nm. As shown in Fig.4, the four-parameter (4-P) model can represent both the emission and the absorption with reasonable accuracy, although it is slightly less accurate than the PCA-based linear model (with dimensionality 12).

Since there are only three images in our setup, it is impossible to estimate the four parameters of an absorption spectra. To resolve this problem, we further observe that the emission and absorption pair of a fluorescent material usually have almost the same length of tail, as illustrated by the representative pair in Fig.3(a). Thanks to the special property of a skew Cauchy distribution mentioned above, we can first fit the four parameter model to the emission spectra so as to find its skewness parameter $\tilde{\omega}$, and then use -$\tilde{\omega}$ as the skewness parameter of its corresponding absorption spectra model. We have also verified that this three-parameter (3-P) model of absorption is of sufficient accuracy, as shown in Fig.4(b), (g) and (h). Admittedly, this low-dimensional model tends to smooth out some high-frequency details of the absorption spectra. However, it should be acceptable, since the absorption spectra is emerged into a scalar coefficient of emission, as shown in eq.(1).

### 3.2 Estimation Method

Based on the model in eq.(16) and the skewness parameter -$\tilde{\omega}$, the absorption spectra can be expressed as

$$a(\lambda|\bar{\lambda}_0,\bar{\gamma},\bar{h};-\tilde{\omega}) = \frac{\bar{h}}{\left[\bar{\gamma}^2+(\lambda-\bar{\lambda}_0)^2\right]}\left\{\frac{1}{\pi}\arctan\left[\frac{-\tilde{\omega}(\lambda-\bar{\lambda}_0)}{\bar{\gamma}}\right]+\frac{1}{2}\right\}, \tag{17}$$

in which $\bar{\lambda}_0$, $\bar{\gamma}$ and $\bar{h}$ are the three unknown parameters. To estimate these three parameters, we can solve the following nonlinear minimization problem

$$\min_{\bar{\lambda}_0,\bar{\gamma},\bar{h}} \left(\int l_1(\lambda)a(\lambda)d\lambda - a_1\right)^2 + \left(\int l_2(\lambda)a(\lambda)d\lambda - a_2\right)^2 + \left(\int l_3(\lambda)a(\lambda)d\lambda - a_3\right)^2, \tag{18}$$

for which we use the standard Gauss-Newton method.

Considering that eq.(18) defines a minimal problem with three variables and three constraints, one might seek to find all the feasible solutions. However, due to the anti-trigonometric function in eq.(17), this is too challenging. By fitting the four-parameter model to the recovered emission spectra, we can find at the same time a reasonable initialization for $\bar{\lambda}_0$, $\bar{\gamma}$ and $\bar{h}$. This initialization is of tremendous benefit to the locally optimal Gauss-Newton method, and makes it work very well for solving eq.(18).

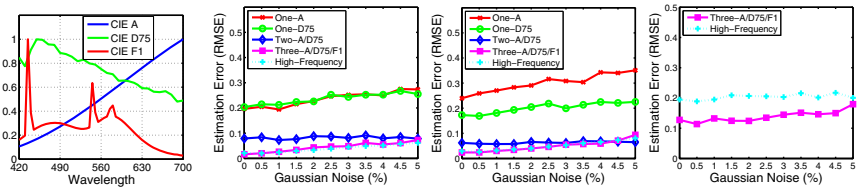


(a) CIE Lights (b) Reflectance (c) Emission (d) Absorption

**Fig. 5.** Estimation accuracy w.r.t. varying noise levels by using synthetic data. (a) shows the three ordinary illumination spectra used in simulation. The estimation error (RMSE) for reflectance, emission and absorption are shown in (b), (c) and (d), respectively. The number (One, Two and Three) in the legend indicates the number of illuminants used.

# 4 Experiment Results

## 4.1 Synthetic Data

Here, we evaluate the accuracy of our proposed methods on synthetic data, and disclose how it compares with that of the state-of-the-art method [9] using specialized high-frequency illuminations.

The standard CIE A, D75 and F1 illumination spectra are used, as shown in Fig.5(a). We randomly select one color from the 18 color patches on the Macbeth color checker as the reflectance spectra. As for the absorption and emission pair, we randomly select one pair from the fluorescent spectra dataset [16] with 181 materials in all. All spectra are normalized such that the maximum value is 1. We add zero-mean Gaussian noise onto the synthesized hyperspectral signals, with standard deviations from 0 to 5% relative magnitude. At each deviation level, we measure the root mean square error (RMSE) of the estimated spectra, with respect to their corresponding ground truth.

By following [9], the period of the high-frequency illuminations is chosen to be 35 nm. We carefully adjust the phase to make sure that the two illuminations are as complementary as possible, while avoiding the singularities when they have the same value.

The average RMSE over 200 independent runs for reflectance and emission are respectively shown in Fig.5(b) and Fig.5(c), from which we can see that our separation method has the same accuracy as [9], although only ordinary illuminants are used. In addition, as illustrated in Fig.5(d), our absorption spectra estimation method is clearly better in accuracy than the heuristic method in [9].

To further validate our analysis on the risk of using one or two ordinary illuminants, we also include them into comparison, as shown in Fig.5(b-c). Even in no presence of noise, the estimation accuracy of using one or two illuminants is not satisfactory. Note that, in the solving process, we have used convex optimization or exhaustive one-dimensional search to preclude any potential influence of local minima. As analyzed in Sec.2.3, the estimation inaccuracy is indeed caused by the dependency between the linear subspace models of reflectance and fluorescent emission.

An interesting observation from Fig.5(b-c) is that, when using two illuminants, the estimation accuracy is higher than using three illumiants in the highly noisy cases, e.g., with 5% relative noise. This is due to that our algorithm for three illuminants does

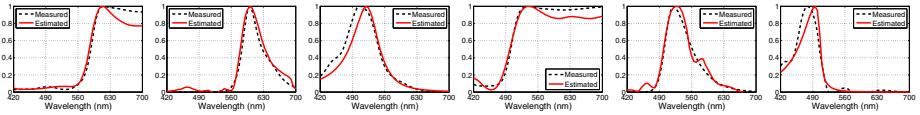


(a) Ref. (Red) (b) Emi. (Red) (c) Abs. (Red) (d) Ref. (Yell.) (e) Emi. (Yell.) (f) Abs. (Yell.)

**Fig. 6.** The estimated reflectance, emission and absorption spectra for the red (a-c) and yellow (d-f) patch in the scene of Fig.1, w.r.t. their respective measured ground truth.

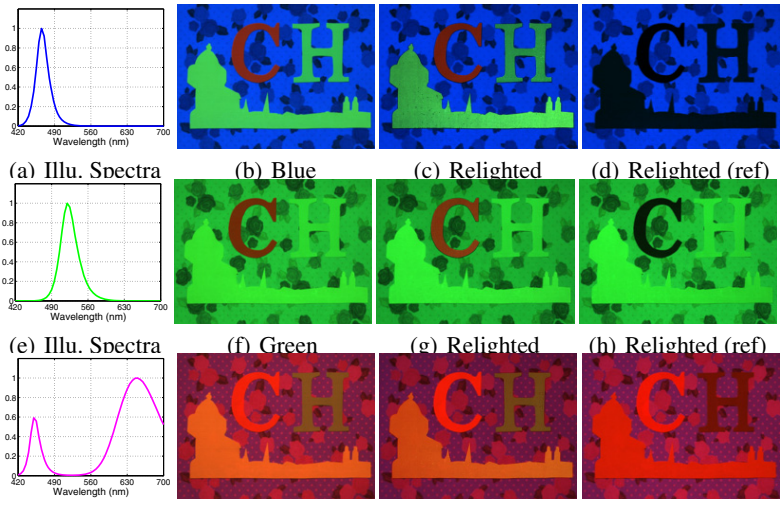


(a) Illu. Spectra (b) Blue (c) Relighted (d) Relighted (ref)

(e) Illu. Spectra (f) Green (g) Relighted (h) Relighted (ref)

(i) Illu. Spectra (j) Pink (k) Relighted (l) Relighted (ref)

**Fig. 7.** Relighting the scene in Fig.1(c) under blue, green and pink color illuminations.

not involve the subspace models in the process of minimizing eq.(3), in order to be relatively fair when comparing with [9]. It is expected that, when the subspace models are embedded into our algorithm, the separation accuracy could be further improved, at the cost of longer running time.

### 4.2 Real Images

We use as lighting sources three ordinary illuminants, including an incandescent, a LED and a fluorescent bulb, as shown in Fig.1(a). Their spectra are presented in Fig.1(b). An EBA JAPAN NH-7 hyperspectral camera is used to capture images in the visible range from 420 nm to 700 nm with an interval of 5 nm. For visualization, all hyperspectral images are shown in RGB.

Given three hyperspectral images, we first separate the fluorescent and reflective components by following the procedures in Sec.2.2, and then estimate the absorption spectra by using the method in Sec.3.2.

As shown in Fig.1(c), we first design a scene with three fluorescent patches, whose reflectance, absorption and emission spectra have been measured. Fig.1(d) and Fig.1(e) show the rendered RGB images of our estimated reflectance and fluorescent emission

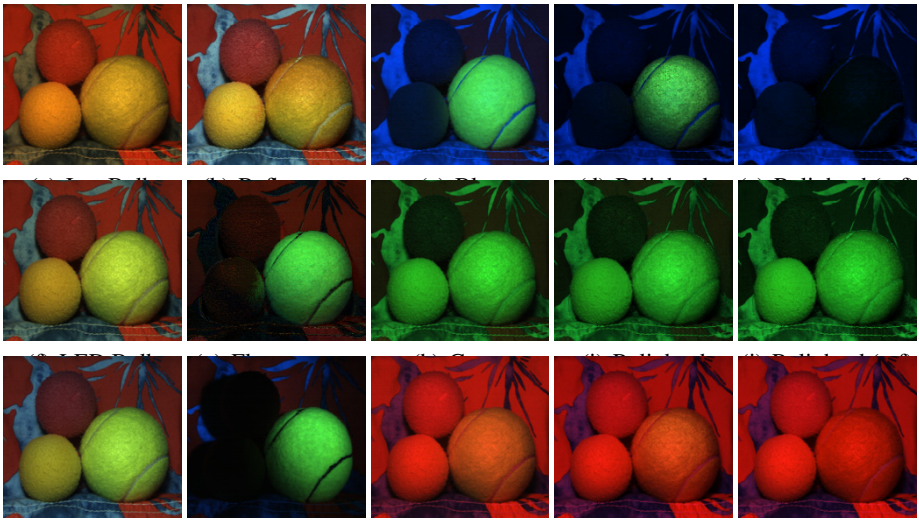

(k) Flu. Bulb (l) UV (m) Pink (n) Relighted (o) Relighted (ref)

**Fig. 8.** Tennis ball and sport shorts scene. The 1st column shows the scene under the three illuminants. Our separation results are shown in the 2nd column, which also includes the scene under near UV light for reference. The 3rd column shows the scene under novel color illuminations, while the 4th and 5th columns include the relighting results with fluorescence and without fluorescence, respectively.

spectra, respectively. By referring to the quantitative comparison in Fig.6, we can see that the estimated spectra are sufficiently close to their corresponding measured ones. As for the estimated reflectance spectra in Fig.6(a) and (d), minor discrepancy occurs in the range from 630 nm to 700 nm. This is caused by low-irradiance of the fluorescent bulb in that range, as shown in Fig.1(b). This low-irradiance problem causes some inaccuracy in the process of posterior white balancing.

Given the full spectra of a fluorescent-reflective scene, we can easily relight the scene under any illumination spectra on the basis of the imaging equation. The relighting results of the scene in Fig.1(c) under blue, green and pink illuminations are shown in Fig.7, from which we can see that accounting for reflectance only would cause poor relighting results, when nontrivial fluorescence is present in the scene.

We have also evaluated our methods on scenes with manmade objects, like the tennis ball and sport shorts scene in Fig.8 and the candle scene in Fig.9. The apparent advantages in relighting results not only reveal the effectiveness of our proposed methods, but also underline the necessity of accounting for fluorescence. In Fig.8(d), the relighted tennis ball assumes nontrivial discrepancy from its ground truth in Fig.8(c). We are speculating that the felty surface of a tennis ball goes somehow beyond the diffuse imaging equation in eq.(1). To further identify the reason and the possible solution is our future work.

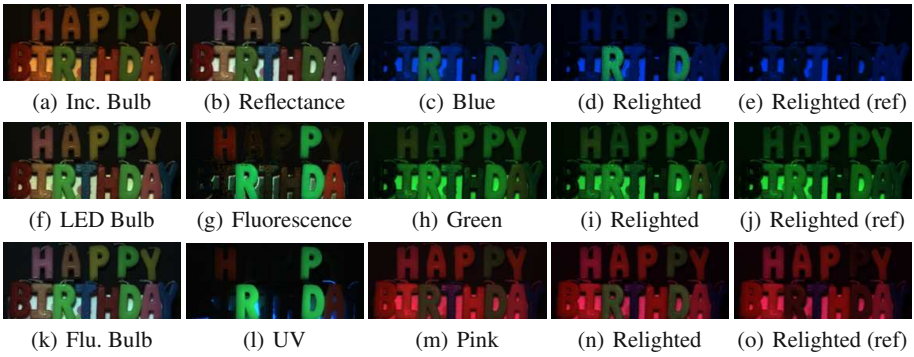

(a) Inc. Bulb (b) Reflectance (c) Blue (d) Relighted (e) Relighted (ref)

(f) LED Bulb (g) Fluorescence (h) Green (i) Relighted (j) Relighted (ref)

(k) Flu. Bulb (l) UV (m) Pink (n) Relighted (o) Relighted (ref)

**Fig. 9.** Candle scene. The scene under various illuminations, as well as the separation and relighting results, have the same layout as in Fig.8.

## 5 Conclusions

We have proposed accurate and effective methods to estimate the full spectra of a fluorescent-reflective scene by using hyperspectral images under ordinary illuminations. We disclosed the linear dependence between the PCA-based linear bases of reflectance and fluorescent emission, and showed that using one or two images is insufficient for accurate reflectance and emission separation. In the presence of three hyperspectral images, we have reformulated the imaging equations into a linear system, and revealed that three wideband and independent illuminants in general are sufficient for the separation task. An elegant convex optimization method was proposed for solving, whose solution can be further polished via a few alternating iterations. As for absorption estimation, we proposed a novel four-parameter nonlinear model to express absorption and emission spectra. Based on this model, an absorption spectra estimation method in the presence of three illuminations was proposed as well. Experiment results have verified the accuracy and effectiveness of our proposed methods.

Considering that the four-parameter model is more discriminative than the linear model, it might benefit the task of separating the fluorescent and reflective components in a single hyperspectral image. We plan to explore this possibility in the future.

## References

1. Alterman, M., Schechner, Y., Weiss, A.: Multiplexed fluorescence unmixing. In: IEEE International Conference on Computational Photography pp. 1–8 (2010)
2. Arnold, B., Beaver, R.: The skew-Cauchy distribution. Statistics & Probability Letters 49(3), 285–290 (2000)
3. Azzalini, A.: The Skew-Normal and Related Families, 1st edn. Cambridge University Press (2014)
4. Barnard, K.: Color constancy with fluorescent surfaces. In: Proc. of the Color and Imaging Conference, pp. 257–261 (1999)
5. Boyd, S., Parikh, N., Chu, E., Peleato, B., Eckstein, J.: Separating the fluorescence and reflectance components of coral spectra. Applied Optics 40(21), 3614–3621 (2001)

6. Boyd, S., Vandenberghe, L.: Convex Optimization, 1st edn. Cambridge University Press (2004)
7. Chane, C., Mansouri, A., Marzani, F., Boochs, F.: Integration of 3D and multispectral data for cultural heritage applications: survey and perspectives. Image and Vision Computing 31(1), 91–102 (2013)
8. Fu, Y., Lam, A., Kobashi, Y., Sato, I., Okabe, T., Sato, Y.: Reflectance and fluorescent spectra recovery based on fluorescent chromaticity invariance under varying illumination. In: IEEE Conference on Computer Vision and Pattern Recognition, pp. 2163–2170 (2014)
9. Fu, Y., Lam, A., Sato, I., Okabe, T., Sato, Y.: Separating reflective and fluorescent components using high frequency illumination in the spectral domain. In: IEEE International Conference on Computer Vision, pp. 457–464 (2013)
10. Han, S., Matsushita, Y., Sato, I., Okabe, T., Sato, Y.: Camera spectral sensitivity estimation from a single image under unknown illumination by using fluorescence. In: IEEE Conference on Computer Vision and Pattern Recognition, pp. 805–812 (2012)
11. Johnson, G., Fairchild, M.: Full-spectral color calculations in realistic image synthesis. IEEE Computer Graphics and Applications 19(4), 47–53 (1999)
12. Kim, S., Zhuo, S., Deng, F., Fu, C., Brown, M.: Interactive visualization of hyperspectral images of historical documents. IEEE Trans. Visualization and Computer Graphics 16(6), 1441–1448 (2010)
13. Lam, A., Sato, I.: Spectral modeling and relighting of reflective-fluorescent scenes. In: IEEE Conference on Computer Vision and Pattern Recognition, pp. 1452–1459 (2013)
14. Leland, J., Johnson, N., Arecchi, A.: Principles of bispectral fluorescence colorimetry. In: Proc. SPIE, vol. 3140, pp. 76–87 (1997)
15. Maloney, L.: Evaluation of linear models of surface spectral reflectance with small numbers of parameters. J. Opt. Soc. Am. A 3(10), 1673–1683 (1986)
16. McNamara, G., Gupta, A., Reynaert, J., Coates, T., Boswell, C.: Spectral imaging microscopy web sites and data. Cytometry Part A 69(8), 863–871 (2006)
17. Park, J., Lee, M., Grossberg, M., Nayar, S.: Multispectral imaging using multiplexed illumination. In : IEEE International Conference on Computer Vision, pp. 1–8 (2007)
18. Parkkinen, J., Hallikainen, J., Jaaskelainen, T.: Characteristic spectra of munsell colors. J. Opt. Soc. Am. A 6(2), 318–322 (1989)
19. Sato, I., Okabe, T., Sato, Y.: Bispectral photometric stereo based on fluorescence. In: IEEE Conference on Computer Vision and Pattern Recognition, pp. 270–277 (2012)
20. Suo, J., Bian, L., Chen, F., Dai, Q.: Bispectral coding: compressive and high-quality acquisition of fluorescence and reflectance. Optics Express 22(2), 1697–1712 (2014)
21. Tominaga, S., Horiuchi, T., Kamiyama, T.: Spectral estimation of fluorescent objects using visible lights and an imaging device. In: Proc. of the Color and Imaging Conference, pp. 352–356 (2011)
22. Treibitz, T., Murez, Z., Mitchell, B.G., Kriegman, D.: Shape from fluorescence. In: Fitzgibbon, A., Lazebnik, S., Perona, P., Sato, Y., Schmid, C. (eds.) ECCV 2012, Part VII. LNCS, vol. 7578, pp. 292–306. Springer, Heidelberg (2012)
23. Zhang, C., Sato, I.: Separating reflective and fluorescent components of an image. In: IEEE Conference on Computer Vision and Pattern Recognition, pp. 185–192 (2011)